IEEE Access
Multidisciplinary ⋮ Rapid Review ⋮ Open Access Journal

Received 30 September 2024, accepted 7 November 2024, date of publication 19 November 2024,
date of current version 30 December 2024.

Digital Object Identifier 10.1109/ACCESS.2024.3502513

RESEARCH ARTICLE

Classification of Skin Lesion With Features Extraction Using Quantum Chebyshev Polynomials and Autoencoder From Wavelet-Transformed Images

FARHATULLAH[1], XIN CHEN[2], (Member, IEEE), DEZE ZENG[1], (Senior Member, IEEE), JIAFENG XU[2], (Student Member, IEEE), RAB NAWAZ[3], (Member, IEEE), AND RAHMAT ULLAH[3], (Member, IEEE)

[1]School of Computer Science, China University of Geosciences, Wuhan 430074, China
[2]School of Automation, China University of Geosciences, Wuhan 430074, China
[3]School of Computer Science and Electronic Engineering, University of Essex, CO4 3SQ Colchester, U.K.

Corresponding authors: Xin Chen (chenxin@cug.edu.cn) and Rahmat Ullah (rahmat.ullah@essex.ac.uk)

ABSTRACT Skin, a vital organ acting as a protective barrier to the external environment, plays a pivotal role in overall human health. Early detection of skin diseases is essential, as untreated conditions can escalate to serious issues such as skin cancer. This study presents an innovative automated system designed for efficient classification of skin lesions, addressing the growing demand for advanced biomedical image analysis. Leveraging the power of Deep Learning, the proposed model incorporates several pre-processing techniques such as wavelet transformations, pooling methods, and normalization to enhance image clarity and remove extraneous artifacts. Two distinct feature extractors are used to extract key features: Quantum Chebyshev polynomials for initial feature extraction, followed by an Autoencoder (AE) for feature refinement and dimensionality reduction. These optimized features are classified using Long Short-Term Memory (LSTM). The experimental evaluation of the proposed model includes analysis with five different optimizers: Adam, RMSprop, SGD, Adadelta, and Adagrad, accross two widely recognized datasets, ISIC2017 and HAM10000. The resutlts reveals that the Adam optimizer consistently yields the highest scores across multiple evaluation matrices. For the ISIC2017 dataset, the model achieves 98.87% accuracy, 98.23% precision, 98.26% recall, F1-score 98.24%, and 98.16% specificity. The HAM10000 dataset exhibits even more remarkable metrics, with 99.58% accuracy, 97.84% precision, 97.49% recall, 97.66% F1-score, and 97.74% specificity. The proposed model surpasses the current state-of-the-art in skin lesion classification and holds the potential to serve as a valuable tool for medical professionals, aiding in the automated classification of skin cancer.

INDEX TERMS Skin lesion classification, deep learning, medical diagnosis, biomedical image analysis, wavelet transformations, quantum Chebyshev polynomials, autoencoders, feature extraction.

I. INTRODUCTION

Skin Cancer (SC) presents a considerable health challenge on a global scale, affecting a substantial portion of the global population. It arises from the unusual growth of melanocyte cells, causing damage to the surrounding skin tissue [1]. There are different types of SC, but the most common ones are melanoma and non-melanoma, which take center stage in SC [2]. Its aggressive nature and rapid metastasis distinguish melanoma and have a significantly higher mortality rate, emphasizing the critical need for its early detection [3]. The two most common types of non-melanoma SC basal cell carcinoma (BCC) and squamous cell carcinoma (SCC) [4]. Melanoma SC demands early

The associate editor coordinating the review of this manuscript and approving it for publication was Donato Impedovo.

detection and is primarily linked to the adverse effects of ultraviolet radiation [5]. Melanoma, BCC, and SCC) are serious skin conditions [4]. Melanoma, in particular, requires early detection and is mainly caused by the harmful effects of ultraviolet radiation [5]. The American Cancer Society has released alarming data predicting over 1 million cases of melanoma to be reported in 2020, with an estimated 6,000 deaths. Similarly, the 19th Skin Cancer Conference highlighted the prevalence of skin melanoma, reporting 300,000 new cases in 2018 alone. These reported cases only offer a partial view of the situation, as recent data in the United States shows an increasing trend in fatalities [6]. This underscores the urgency of advancing our understanding of this formidable disease and improving early detection methods. According to the World Health Organization (WHO), 60,000 individuals die annually from sun exposure, with 48,000 deaths caused by melanoma [7]. If left undetected or untreated in its early stages, melanoma can spread to vital organs such as the brain, liver, bones, and lungs, causing significant suffering for patients with skin cancer [8]. Therefore, early detection of melanoma is crucial in diagnosing skin cancer. Over the past few decades, the biopsy procedure has been the cornerstone for examining skin cancer in the initial stages, providing reliable results.

Nevertheless, these methods still rely on the expertise of dermatologists for accurate cancer detection. In recent years, dermatologists have increasingly embraced microscopic and dermoscopy images as valuable aids in the diagnosis of SC [9]. These images are meticulously examined visually. However, dermatologists' visual inspection and appraisal of SC are time-consuming and labor-intensive procedures [10], and requires a high skill level [11]. With the advancement of technology, the classification of medical images has gained increasing significance, particularly in the context of Computer-Aided Diagnosis (CAD) [12]. Dermatologists, facing the growing complexity of physical screenings, have increasingly turned to CAD systems as valuable allies in the diagnosis of SC [13]. CAD methods empower dermatologists to make swifter and more precise decisions regarding SC screenings [14]. Importantly, CAD techniques have demonstrated a distinct advantage over human methods, offering both speed and accuracy [15], [16]. However, it's crucial to emphasize that potential image abnormalities, such as bubbles, hair, blood vessels, and oils within skin lesion images, can present difficulties in classification endeavors [17]. To avoid this problem, the CAD system encompasses several pivotal stages, including contrast enhancement, segmentation, feature extraction, and classification through machine learning (ML) and Deep learning (DL) algorithms. The existing body of research highlights the development of various contrast enhancement techniques, including color adjustments, hybrid filters, and blur reduction methods utilizing dark channel approaches [18]. Contrast enhancement is pivotal in improving the accuracy of lesion classification, which is a critical precursor to reliable feature extraction [19]. Numerous techniques for lesion segmentation have been explored, such as clustering, saliency-based region growth, and thresholding [20]. Traditionally, images are used directly for feature extraction in a conventional manner. However, computer vision researchers have successfully addressed the issue of irrelevant features by integrating feature selection methods [20]. These techniques intelligently select the most pertinent features from the initially extracted pool, resulting in a significant reduction in computational complexity [21], [22]. This seamless incorporation of CAD methodologies presents a promising avenue for more effective and efficient SC diagnosis. The use of DL based techniques have played a transformative role in enhancing skin lesions classification accuracy [23].

A. LIMITATION IN PREVIOUS WORK

In recent years, advancements in the field of skin lesion analyses have experienced a surge in research, lagly driven by the widespread adoption of DL techniques. While these efforts are commendable, several critical challenges remain in this domain, demanding further investigation. These challenges includes issues such as unbalanced datasets, low-contrast and noisy skin lesions, and the number of features across different classes. This study seeks to address these challenges by introducing a robust preprocessing strategy aimed at balancing datasets, enhancing image contrast, and removing noise from skin lesion images. Accurate feature classification at this stage is crucial, as it directly influences the quality of the final diagnosis. Unlike conventional methods, this research adopts a two-step process: first, features are extracted, and then these features are refined to extract meaningful information while reducing dimensionality. Using this approach, the study aims to significantly improve the accuracy and reliability of multi-class skin lesion classification, offering a potentially valuable contribution to the field of dermatology.

B. OBJECTIVES OF THE PROPOSED WORK

The primary aim of this study is to develop a sophisticated, multi-class skin lesion classification model that addresses key limitations in existing research, particularly the challenges posed by uncertainty in lesion classification. Skin lesion images often exhibit high variability in appearance due to differences in color, texture, shape, and size, as well as the presence of artifacts and noise. These factors contribute to overlapping features among different lesion types, making accurate classification a complex task.

To tackle these uncertainties, our proposed model integrates advanced preprocessing and feature extraction techniques directly into its structure. By employing Quantum Chebyshev Polynomials (QCHPs) for initial feature extraction, we aim to capture essential and nuanced features that are most relevant to distinguishing between lesion types. The subsequent use of an Autoencoder for dimensionality reduction and feature refinement helps in preserving critical information while eliminating redundancies and noise. This combination enhances the model's ability to focus on the

most discriminative features, thereby reducing uncertainty in classification outcomes. The objectives are as follows:

- Implement data augmentation techniques such as, flipping, zooming, contrast adjustments, translations, brightness changes, and rotations to address dataset imbalance and improve classification accuracy.
- Develop a robust preprocessing approach to enhance image clarity and eliminate artifacts, allowing for more precise lesion analysis.
- Utilize Quantum Chebyshev polynomials (QCHPs) for initial feature extraction, followed by dimensionality reduction and refinement using an Autoencoder.
- Classify refined features using LSTM networks to leverage their sequential memory capabilities.
- Conduct comprehensive experiments using five optimization algorithms (Adam, RMSprop, SGD, Adadelta, and Adagrad) to test the model's performance.
- Evaluate the model's effectiveness through a wide range of performance metrics to ensure a thorough assessment.
- Benchmark the proposed method against state-of-the-art models to highlight its advantages in multi-class skin lesion classification.

The structure of the paper is as follows: Section II presents a comprehensive literature review. Section III details the study's methodology, including preprocessing, feature extraction, and the use of LSTM for classification. Section IV summarizes the experimental phase, covering the datasets, optimizers, and performance metrics used to evaluate the proposed model. Finally, Section V concludes with key insights, discusses the research implications, and outlines potential directions for future work in multi-class skin lesion classification.

II. LITERATURE REVIEW

A model was proposed that achieved promising results in skin lesion recognition without relying on filtering or feature extraction techniques [24]. Image preprocessing methods such as Local Binary Pattern (LBP) and GLCM, combined with fuzzy c-clustering, were employed in a system that showed particularly strong results in skin lesion identification [25]. Similarly, a Conditional Random Field (CRF) module was introduced to enhance lesion boundaries and contours, combined with a convolutional network optimized through hyper-parameter tuning to deliver commendable outcomes [26].

Data augmentation techniques were developed to balance lesion types within the dataset, utilizing LSTM and MobileNet V2 for effective classification and detection of skin diseases while maintaining computational efficiency [27]. The effect of image size on skin lesion classification was evaluated, and an ensemble strategy was employed, combining six different scales and three fine-tuned CNNs to enhance classification accuracy [28]. Another study adapted the whale optimization technique, which was used to fine-tune CNN parameters, improving performance in matching network outputs with target outputs [29]. A novel methodology integrating elements of NL and DL automated skin lesion segmentation was proposed based on a ''divide and conquer'' strategy in [30].

An automated segmentation network specifically designed for skin lesions, incorporating separable depth-wise convolution to reduce parameter complexity, was introduced to enhance segmentation efficiency [31]. Simillary, the AlexNet model was used with randomized weights in the final three layers, and was evaluated on the ISIC 2018 dataset as one of the most recent public resources for skin lesion classification [32]. In another approach, Support Vector Machines (SVM) and Radial Basis Function (RBF) were employed to classify three distinct skin lesion classes, utilizing a method called fractal-based regional texture analysis (FRTA) to extract various features such as color, texture, and shape [33]. Additionally, integrating gradient information with LBP improved the classification of skin lesion segmentation masks [34], while another system used fuzzy histogram thresholding for effective lesion segmentation [35].

A comprehensive model based on the ABCD rule was formulated for partitioning and classifying skin images, involving pre-processing, Region of Interest (ROI) identification, feature extraction, and classification [36]. The MASK-RCNN model was introduced for skin lesion segmentation, with a DenseNet model employed for classification, achieving notable success in both tasks [37]. Earlier work by the same team developed an automated system for skin lesion classification by leveraging pre-trained Transfer Learning (TL) models for feature extraction, followed by principal component analysis (PCA) for feature selection and SVM for classification [38]. A more recent study introduced a framework combining MASK-RCNN for segmentation with a ResNet50 network, and employed a 24-layer CNN architecture for lesion classification [39].

To classify melanoma, a hybrid approach combining Artificial Neural Networks (ANN) and Logistic Regression (LR) was employed, focusing on lesion thickness as a key metric [40]. Another study developed a system using CNN along with local descriptor encoding to classify dermoscopic images, extracting features with ResNet101 and ResNet50 and applying a Fisher vector for global image representation before classification with SVM [41]. The VGG16 model was fine-tuned for classification of the HAM10000 dataset, achieving 89.09% accuracy [42], with follow-up studies exploring the application of Xception and MobileNet models on the same dataset [43], [44]. A hybrid model combining U-Net for segmentation and CNN for classification was proposed, and its performance was evaluated using the HAM10000 dataset, with analysis conducted using Adam and Adadelta optimizers [45].

A practical method for identifying skin cancers through dermoscopy images enhances accuracy in distinguishing between different classes. Using Swarm Intelligence (SI) techniques, dermoscopy images are analyzed to detect skin lesions. The Grasshopper Optimization algorithm delivers

optimal segmentation results. Based on these segmented images, the Speeded-Up Robust Features (SURF) method is employed to extract features. This approach is validated on three datasets: ISIC-2017, ISIC-2018, and PH-2 databases [46]. Furthermore, individual models have limited accuracy in detection, but combining their decisions through ensemble learning improves performance. This approach develops an ensemble of deep learners, including VGG, CapsNet, and ResNet, to enhance skin cancer detection accuracy [47]. Another study employed two autoencoders spatial and Fast Fourier Transform (FFT) to capture spatial and frequency-based textural features from skin lesions. By incorporating attention modules and using an Extreme Learning Machine (ELM) for classification, the system effectively detects skin malignancies based on features extracted from the autoencoders' bottleneck layers [48]. A similar study aimed to develop and select the best model for skin cancer feature extraction and classification. Feature reduction was performed using two Grey Wolf Optimizer (GWO) algorithms alongside the original features. The optimal model was identified through a multicriteria decision-making approach, ranking alternatives based on perimeter similarity (RAPS) [49].

A Wavelet Transform-based Deep Residual Neural Network (WTDRNNet) was introduced for classification using the ISIC2017 and HAM10000 datasets. This model enhanced image details through wavelet transformation, pooling, and normalization, and utilized recurrent neural networks (RNN) combined with transfer learning for feature extraction [50]. In summary, skin lesion classification has advanced significantly through a wide array of ML and DL approaches, particularly on the HAM10000 and ISIC-2017 datasets [51], [52], [53], [54], [55], [45], [50], resulting in considerable improvements in classification accuracy and methodology.

III. MATERIALS AND METHOD

A. DATASETS

The comprehensive schematic of the proposed approach is shown in Fig 1. Two publicly available datasets of dermoscopic skin lesion images: ISIC-2017 [50] and HAM10000 [56] are used in this study. The ISIC-2017 dataset consists of a collection of 2750 dermoscopic images and contains three classes of skin lesions: benign (Nev), melanoma (Mel), and seborrheic keratosis (Seb).

The HAM10000 dataset consists of 10,015 dermoscopic images divided into seven different classes, namely Melanocytic nevi (Nv), Melanoma (Mel), Benign keratosis (Bkl), Basal Cell Carcinoma (Bcc), Actinic keratosis (Ak), Vascular Lesions (Vasc), and Dermatofibroma (Df).

B. DATA AUGMENTATION

Both the ISIC-2017 and HAM10000 datasets exhibit an imbalanced distribution of images across different classes. To mitigate this issue and improve the robustness of our proposed model, data augmentation techniques were applied.

TABLE 1. Number of images in each dataset before and after augmentation.

Dataset	Class	Orignal images	Augmented images
ISIC-2017	Nev	1843	1843
	Mel	521	1563
	Seb	386	1158
HAM10000	Nv	6705	6705
	Mel	1113	6678
	Bkl	1099	6594
	Bcc	514	3084
	Ak	327	1962
	Vasc	142	852
	Df	115	690

These techniques included operations such as flipping, zooming, contrast adjustments, translations, brightness modification, and rotations. As a result, the data for minority classes increased nearly threefold in ISIC-2017 and sixfold in HAM10000, significantly expanding their original sizes. The number of images after augmentation in ISIC-2017 is 4564, and HAM10000 is 26565, as detailed in Table 1. From the augmented datasets, 70% of images are used for training and 30% for testing.

C. PRE-PROCESSING

In the pre-processing stage, operations are implemented to eliminate the noise and artifacts from images. First, a 2D Discrete Wavelet Transform (2D DWT) as in Eq. (1) is applied to the original images [50], decomposing them into four distinct components: Low-Low, Low-high, High-Low, and High-high bands. Each component consists of a different frequency within the images. The low-low (LL) component is then selected, essentially approximating the original image and preserving vital information while reducing extraneous details. Subsequently, max pooling as in Eq. (2) and normalization in Eq. (3) are employed for dimension reduction and pixel scaling, respectively. This carefully curated sequence of operations produces a refined image, enhancing essential features while removing unwanted elements. The enhanced image is then subjected to the same process again, further improving its quality for subsequent analysis phases.

$$W(x, y; a, b) = \int \int I(x, y)\Psi\left(\frac{x-a}{b}, \frac{y-a}{b}\right) dx\, dy \quad (1)$$

a and b represent the scaling and translation parameters and Ψ is the mother wavelet.

$$p_{\max}(i, j) = \max_{p,q \in N(i,j)} I(p, q) \quad (2)$$

$p_{\max}(i, j)$ represents the value located at position (i, j) within the pooled image, with $N(i, j)$ representing the set of pixels within the $k \times k$ neighborhood.

$$I_{\text{normalized}}(x, y) = \frac{I\langle x, y\rangle - \min(I)}{\max(I) - \min(I)} \quad (3)$$

$I_{\text{normalized}}(x, y)$ represents the normalized pixel value at the position (x, y), while $\min(I)$ and $\max(I)$ represent pixel values in image.

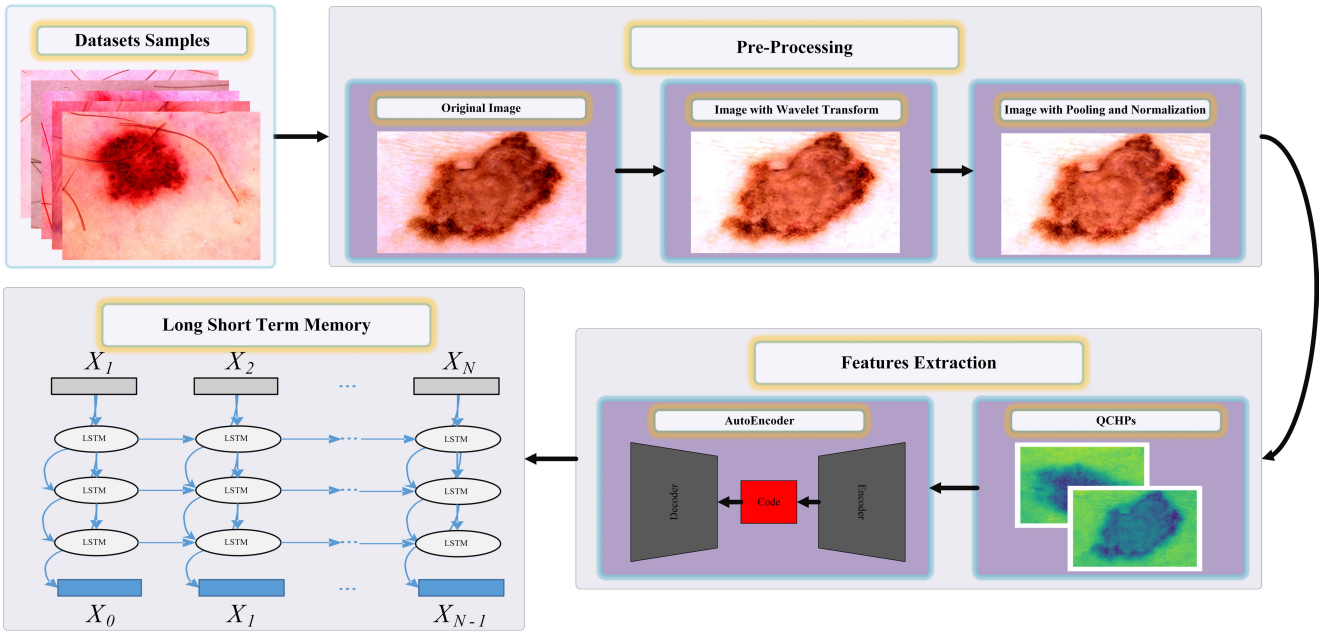

FIGURE 1. Framework of the proposed methodology for skin lesion classification using deep learning techniques. The figure illustrates the complete process starting from the dataset samples through various stages of preprocessing, including wavelet transformation and image normalization. Subsequently, feature extraction is performed using two methods: an Autoencoder and quantum Chebyshev polynomials (QChP). The extracted features are then processed using LSTM network to classify the skin lesions effectively.

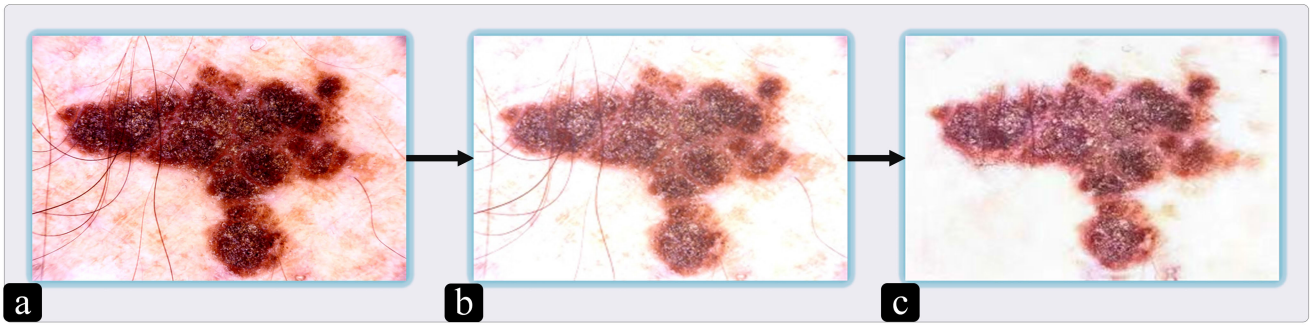

FIGURE 2. Displays the outcomes of the pre-processing steps: (a) the original input image, (b) the image post-wavelet Transform, and (c) the results after pooling and normalization.

D. FEATURE EXTRACTION

In this study, we utilized a two-step feature extraction process that combines QChPs and an Autoencoder to identify and reduce relevant features from the dataset. This method ensures that only the most significant information is retained for classification. We determined the cut-off degree for feature selection through both empirical testing and theoretical considerations, setting it at 4. This degree strikes an optimal balance between feature relevance and model complexity, resulting in strong performance across various metrics, including classification accuracy, precision, recall, and F1-score. Higher-degree polynomials in QChPs tend to introduce noise and unnecessary complexity, while lower degrees may fail to capture essential information. The selected features were then processed through an Autoencoder, which further compressed the feature set while preserving key information. This combined approach facilitated efficient feature extraction and enhanced model performance, as confirmed by feature importance analysis. Additionally, further details on the theoretical aspects of the QChPs and the Autoencoder are provided below.

1) QUANTUM CHEBYSHEV POLYNOMIALS

Quantum calculus, often referred to as q-calculus, extends classical mathematical concepts using a base parameter q. In this framework, traditional operations such as differentiation and integration are redefined, providing a new lens through which to explore and manipulate functions. The Quantum Chebyshev Polynomials (QChPs) are derived within this framework, offering a novel approach to analyzing features in image processing.

The q-exponential function, denoted as $e_q(x)$, is fundamental in q-calculus. It generalizes the exponential function using the q-factorial, defined as $[n]_q!$, which in turn is based on the q-Pochhammer symbol $(q;q)_n$. Equation (4) presents $e_q(x)$:

$$e_q(x) = \sum_{n=0}^{\infty} \frac{x^n}{[n]_q!} \tag{4}$$

This representation captures the essence of exponential growth modified by the quantum parameter q, which adjusts the rate and form of the function's expansion.

The q-Pochhammer symbol, $(q;q)_n$, appearing in Eq. (5), is pivotal for defining factorial-like products in q-calculus. It is used extensively in the computation of q-series and other quantum functions:

$$(q;q)_n = \prod_{k=0}^{n-1}(1-q^k) \tag{5}$$

The Chebyshev polynomials of the first kind, $T_n(x)$, are orthogonal polynomials arising from the recurrence relation shown in Eq. (6):

$$\begin{cases} T_0(x) = 1 \\ T_1(x) = x \\ T_{n+1}(x) = 2xT_n(x) - T_{n-1}(x) \end{cases} \tag{6}$$

These polynomials are crucial for approximating and interpolating functions in numerical analysis and are adapted here for the quantum setting.

The ordinary generating function for $T_n(x)$ is specified in Eq. (7), offering a compact form for the entire polynomial series:

$$\sum_{n=0}^{\infty} T_n(x)t^n = \frac{1-tx}{1-2tx+t^2} \tag{7}$$

Additionally, the exponential generating function, which weighs the polynomials by factorials, is elaborated in Eq. (8), showing its dependency on the exponential function. The function depends on t and x, with the terms involving $\sqrt{x^2-1}$ handling the behavior of the polynomials in different intervals. In Eq. (9) the same expression is simplified further to involve the hyperbolic cosine function (cosh):

$$\sum_{n=0}^{\infty} T_n(x)\frac{t^n}{n!} = \frac{1}{2}\left(e^{t(x-\sqrt{x^2-1})} + e^{t(x+\sqrt{x^2-1})}\right) \tag{8}$$

$$e^{tx}\cosh(t\sqrt{x^2-1}) \tag{9}$$

By integrating the quantum parameter into the Chebyshev polynomials, we obtain the QChP, outlined in Eq. (10). Here, the factorial is replaced by a q-factorial, denoted as $[n]_q!$, which modifies the polynomial's structure to include the quantum parameter q. The inclusion of q introduces a broader range of behavior, making the function sensitive to quantum effects and discontinuities that are not captured by traditional Chebyshev polynomials. In Eq. (11), $[n]_q$ represents the quantum number, modifying classical integers with the quantum parameter q. The summation $\sum_{k=0}^{n}$ expands the polynomial, with each term influenced by the index k. The factor $(-2)^k$ introduces alternating signs, which affect the polynomial's oscillatory behavior. The quantum factorials $[n+k-1]_q!$, $[n-k]_q!$, and $[2k]_q!$ scale each term, while $(1-x)^k$ modulates the polynomial based on the variable x, capturing both local continuity and discontinuity in the function.

$$\sum_{n=0}^{\infty}[T_n]_q(x)\frac{t^n}{[n]_q!} = \frac{1}{2}\left(e_q^{t(x-\sqrt{x^2-1})} + e_q^{t(x+\sqrt{x^2-1})}\right) \tag{10}$$

$$[T_n]_q(x) = [n]_q \sum_{k=0}^{n}(-2)^k \frac{[n+k-1]_q!}{[n-k]_q![2k]_q!}(1-x)^k \tag{11}$$

The final step in utilizing QChPs for feature extraction is detailed in Eq. (12), where each pixel's value is considered under the quantum framework, thus enabling a nuanced analysis of textural and morphological details:

$$[T_n]_q(x_{k,l}) = \sum_{i=1}^{k}\sum_{j=1}^{1}\left(x_{k,l} - \frac{2^n(q^n-1)}{q^{2n}-1}\right) \tag{12}$$

2) AUTOENCODER

In the domain of skin lesion analysis, AEs are powerful tools for autonomously acquiring and refining relevant image features, effectively reducing dimensionality while preserving essential attributes [57]. The core concept of autoencoders involves transforming input data into a lower-dimensional representation via an encoder network and then reconstructing the original data through a decoder network. This iterative process minimizes reconstruction error, enabling the network to learn and capture the most significant features of the input images. For skin lesion feature extraction, this process can be divided into two main phases: encoding and decoding. In the encoding phase, the input image passes through multiple neural network layers—collectively referred to as the encoder. Each layer progressively extracts more abstract and critical features from the image. Mathematically, this process is represented in Equation 13.

$$h_i = f(W_i h_{i-1} + b_i) \tag{13}$$

where h_i represents the activation function at layer i and f, W_i is the weight matrix, h_{i-1} is the output from the previous layer, and b_i signifies the bias term.

This is a continuous iterative process until the input image is transformed into a lower-dimensional representation, similar to a compressed feature vector. In the subsequent decoding phase, the network reconstructs the original input image from this compressed representation. This task is executed through another set of layers, referred to as the decoder, with the primary objective of minimizing the disparity between the reconstructed image and the input image. The mathematical representation of the reconstruction

process is shown in Equation 14.

$$r_i = g(W_i' r_{i-1} + b_i') \tag{14}$$

where r_{i-1} represents the reconstructed activations at layer i, g is the activation function, W_i' is the decoder weight matrix, r_{i-1} is the output from the previous decoder layer, and b_i' is the decoder bias term.

E. CLASSIFICATION

LSTM, a specialized type of RNN, tackles the challenging task of processing long-range dependencies in sequential data. Unlike conventional RNNs, which struggle with the ''vanishing gradient problem,'' LSTM includes memory cells and gates to effectively retain and utilize important information across extended sequences. Each gate plays a crucial role in regulating information flow within an LSTM, consisting of three primary gates: the input gate, which allows new information to enter; the forget gate, which decides the relevance of existing information; and the output gate, which manages the transfer of information to the next sequence step. This intelligent mechanism empowers LSTM to retain essential data while discarding irrelevant elements, rendering it exceptionally adept at discerning intricate patterns within sequences. Through the utilization of these memory cells and gates, as elucidated by Eq. (15-20), LSTMs can tackle intricate challenges that conventional RNNs struggle with. Consequently, LSTMs find extensive applicability in tasks such as natural language understanding, speech recognition, and predictive analysis of future data patterns. In this research, LSTM is harnessed to enhance the classification analysis of SC, with the primary objective of improving accuracy and reliability.

$$f_t = \sigma_h(W_f \cdot x_t + u_f \cdot h_{t-1} + b_f) \tag{15}$$

In Eq. (15), the forget gate f_t assumes a critical function in determining which information from the prior cell state ought to be retained or discarded. It considers both the input data x_t and the preceding hidden state h_{t-1} and learned weights and biases to generate a value ranging from 0 to 1, with 0 representing complete forgetting and 1 representing complete retention.

$$i_t = \sigma_h(W_i \cdot x_t + u_i \cdot h_{t-1} + b_i) \tag{16}$$

In Eq. (16), the input gate i_t is responsible for choosing which new data to add to the cell state. Like the forget gate, it takes the input data into account x_t, the previous hidden state h_{t-1}, and learned weights and biases to produce values between 0 and 1.

$$o_t = \sigma_h(W_o \cdot x_t + u_i \cdot h_{t-1} + b_o) \tag{17}$$

In Eq. (17), the output gate o_t dictates which information from the cell state should be utilized to calculate the hidden state at present step h_t. Similar to the previous gates, it utilizes the sigmoid function to generate values ranging from 0 to 1.

$$\tilde{C}_t = \sigma_h(W_c \cdot x_t + u_i \cdot h_{c-1} + b_C) \tag{18}$$

In Eq. (18), the candidate cell state $\tilde{C}_t$ represents new information that can be incorporated into the cell state. It is calculated using the same input data as the previous hidden state and weights as the gates. The sigmoid activation function ensures that it is a value between -1 and 1.

$$C_t = f_t \odot c_{t-1} + i_t \odot \tilde{C}_t \tag{19}$$

In Eq. (19), the cell state C_t is updated by removing information indicated by the forget gate f_t from the previous cell state c_{t-1} and adding the new information provided by the input gate i_t and the candidate cell state $\tilde{C}_t$.

$$h_t = o_t \odot \sigma_h(C_t) \tag{20}$$

Lastly, in Eq. (20), the hidden state h_t At the current time step, the output gate o_t modulates the cell state C_t by passing it through the sigmoid activation function. This resulting hidden state serves as the LSTM's output at time step t and is employed in the classification process of skin lesion analysis.

Following the discussion on LSTM networks, it is crucial to highlight the specific architectures developed for the classification tasks associated with the ISIC and HAM10000 datasets. These architectures were meticulously designed to leverage the nature of the data, optimizing the models for effective classification.

The architecture for the ISIC dataset, as shown in Table 2, includes an LSTM layer to capture the sequential dependencies in the extracted feature vectors, which aids in the precise classification of skin lesions. Additionally, dropout layers are implemented to reduce overfitting during training.

TABLE 2. Architecture of the proposed model for the ISIC dataset.

Dataset	Layer Type	Output Shape	Parameters
ISIC	Input Layer	(32, 64)	0
	LSTM Layer	(32, 64)	33,280
	Dropout Layer (0.2)	(32, 64)	0
	Dense Layer 1	(32, 64)	4,160
	ReLU Activation	(32, 64)	0
	Dropout Layer (0.5)	(32, 64)	0
	Dense Layer 2	(32, 3)	195
Total Parameters			**37,635**

In contrast, the architecture for the HAM10000 dataset, as shown in Table 3, includes two LSTM layers. This design allows the model to effectively learn complex patterns from the larger dataset, significantly improving classification accuracy. Furthermore, dropout layers are incorporated to further mitigate the risk of overfitting.

The selection of LSTM network for this research was driven by several key factors, particularly considering the nature of skin lesion classification. First, handling temporal dynamics is crucial, as skin lesion analysis often requires tracking changes over time, especially in sequential patient follow-up data. LSTMs are well-suited for tasks that involve understanding these time-based patterns. Their superior capacity for retaining long-term dependencies makes them ideal for maintaining historical accuracy in lesion

TABLE 3. Architecture of the proposed model for the HAM10000 dataset.

Dataset	Layer Type	Output Shape	Parameters
HAM10000	Input Layer	(32, 64)	0
	LSTM Layer 1	(32, 128)	99,840
	Dropout Layer (0.2)	(32, 128)	0
	LSTM Layer 2	(32, 64)	49,408
	Dropout Layer (0.5)	(32, 64)	0
	Dense Layer 1	(32, 128)	8,320
	ReLU Activation	(32, 128)	0
	Dense Layer 2	(32, 7)	903
Total Parameters			**158,471**

progression, a challenge where other models might falter without frequent retraining or complex reconfiguration.

Additionally, LSTMs have a strong track record in domains such as natural language processing and speech recognition, where sequential pattern recognition is essential. Their flexibility in tuning for specific data types, including high-resolution images, ensures robust performance with minimal trade-offs in training time or accuracy—both critical in the diverse field of dermatological imaging. While newer models like N-Beats and DeepAR offer promising forecasting capabilities, they are primarily designed for time-series prediction rather than the intricate pattern recognition and classification required in dermatological applications.

F. MODEL EVALUATION

The performance metrics for evaluating the classifier's effectiveness involve four key components: true positive (TP) denotes accurately classified positive instances, while true negative (TN) indicates correctly classified negative instances. False positive (FP) considers instances where positive cases are incorrectly classified, and false negative (FN) reflects the misclassification of negative cases.

Accuracy formulated in Eq. (21) serves as a vital performance measure, providing an overall assessment of the classifier's correctness. This metric is computed by dividing the number of accurate predictions by the total number of predictions made, showcasing the model's capability to classify data accurately.

$$\text{Accuracy} = \frac{TP + TN}{TP + TN + FP + FN} \tag{21}$$

Precision, formulated in Eq. (22), is another essential measure that evaluates the classifier's ability to consistently predict and evaluates the consistency of results when testing a single sample multiple times, indicating the classifier's accuracy in predicting positive class data sample.

$$\text{Precision} = \frac{TP}{TP + FP} \tag{22}$$

Recall, as formulated in Eq. (23), is a classification measure that assesses how effectively relevant results are retrieved. It quantifies the ratio of all positive class data samples correctly predicted as positive by the classifier.

$$\text{Recall} = \frac{TP}{TP + FN} \tag{23}$$

The F1-score, as formulated in Eq. (24) derived from precision and recall, represents *a* weighted average of these two metrics. Its values range between 0 and 1, with 1 signifying the best performance and 0 the worst.

$$\text{F1 Score} = \frac{2 \cdot \text{Precision} \cdot \text{Recall}}{\text{Precision} + \text{Recall}} \tag{24}$$

Specificity, also known as the true negative rate and formulated in Eq. (25), complements sensitivity by focusing on the accurate identification of negative cases. It evaluates the model's capacity to classify instances as negative when they are indeed negative correctly.

$$\text{Specificity} = \frac{TN}{TN + FN} \tag{25}$$

IV. EXPERIMENTAL RESULTS

The experiments for this study were carried out on an HP Omen laptop featuring a robust Intel Core i9 processor and an NVIDIA GeForce RTX 4060 GPU. This hardware configuration enabled efficient processing of DL tasks, greatly improving both the training and inference times of the proposed models. The model was developed using TensorFlow 2.0, with Keras serving as the backend framework. Wavelet transformations were performed using PyWavelets, while NumPy and Scikit-learn were used for data preprocessing and performance evaluation, respectively.

A. RESULTS

Initially, the model was tested using the ISIC-2017 dataset, employing key performance metrics such as accuracy, specificity, recall, precision, and F1-score. A range of optimizers, including Adam, Adagrad, RMSprop, SGD, and Adadelta, was used for experiments with the ISIC-2017 dataset. The experiments maintained a consistent batch size of 64 and involved training for 20 epochs.

Results for the ISIC-2017 dataset, presented in Table 4 and Fig. 3. The proposed model achieved the highest accuracy of 98.87% using the Adam optimizer. While using the RMSprop and SGD optimizer, the accuracy was slightly reduced to 97.76% and 97.13%, respectively. In contrast, the Adadelta and Adagrad optimizers exhibited comparatively lower performance, yielding accuracy scores of 94.50% and 93.23%, respectively. These outcomes underscore the effectiveness of the model, with Adam emerging as the optimal choice among the optimizers.

The confusion matrices of the proposed model, showcasing its performance on the ISIC-2017 dataset with the best results, are presented in Fig. 4 (a-e). Using the Adam optimizer, the Melanoma (Mel), Nevus (Nev), and Seborrheic Keratosis (Seb) classes achieved the True Positive (TP) rate of 98.93%, 94.19%, and 97.69%, respectively. Fig. 4 (a) through 4 (e) provides a detailed breakdown of the confusion matrices corresponding to the Adam, Adagrad, RMSprop, SGD, and Adadelta optimizers, respectively.

The results of the HAM10000 dataset are presented in Table 5 and Fig. 5. The results show the performance of

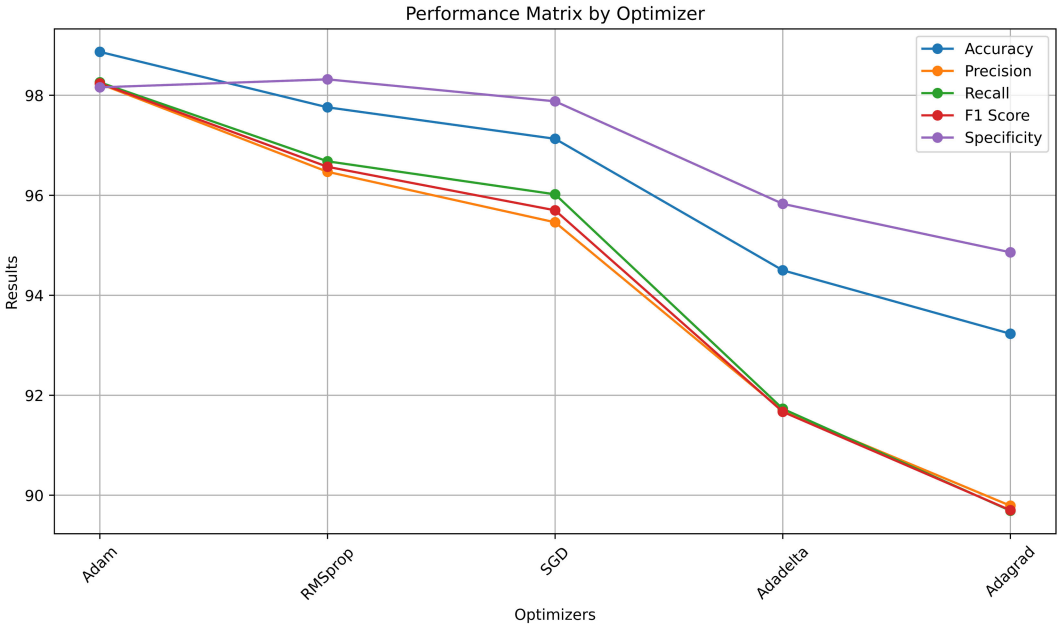

FIGURE 3. Graphical representation of the proposed QChPs-AE-LSTM model with various optimizers on the ISIC-2017 dataset.

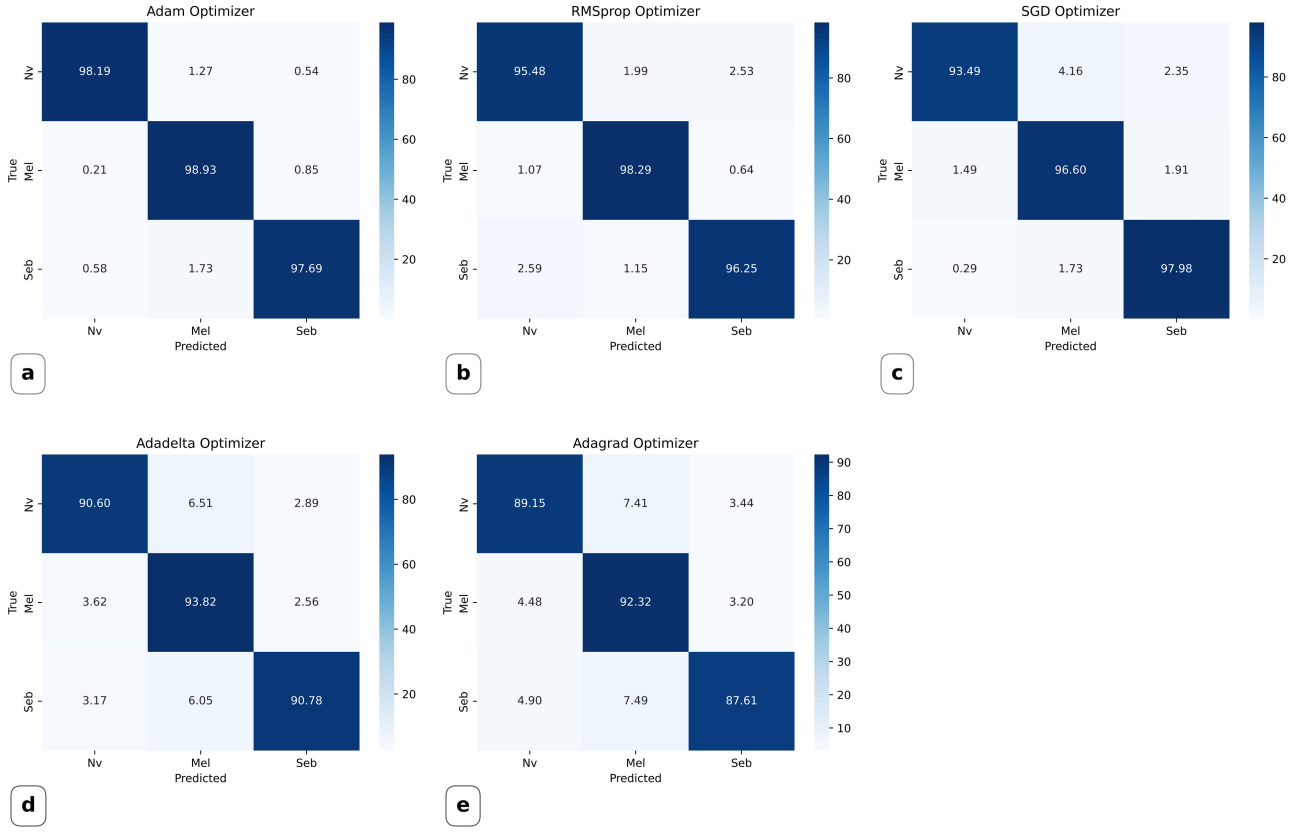

FIGURE 4. The confusion matrix displays classification results for (a) Adam optimizer, (b) RMSprop optimizer, (c) SGD optimizer, (d) Adadelta optimizer, and (e) Adagrad optimizer using ISIC-2017 dataset.

TABLE 4. Results from the proposed QChPs-AE-LSTM model with various optimizers on the ISIC-2017 dataset.

Proposed Methodology	Optimizer	Accuracy (%)	Precision (%)	Recall (%)	F1 Score (%)	Specificity (%)
QChPs-AE-LSTM	Adam	98.87	98.23	98.26	98.24	98.16
	RMSprop	97.76	96.47	96.68	96.57	98.32
	SGD	97.13	95.46	96.02	95.70	97.88
	Adadelta	94.50	91.69	91.73	91.67	95.83
	Adagrad	93.23	89.79	89.69	89.70	94.86

TABLE 5. Results from the proposed QChPs-AE-LSTM model with various optimizers on the HAM10000 dataset.

Proposed Methodology	Optimizer	Accuracy (%)	Precision (%)	Recall (%)	F1 Score (%)	Specificity (%)
QChPs-AE-LSTM	Adam	99.58	97.84	97.49	97.66	97.74
	RMSprop	99.07	94.38	93.11	93.72	99.43
	SGD	98.45	89.19	90.45	89.78	99.08
	Adadelta	98.53	90.12	91.39	90.72	99.13
	Adagrad	98.41	88.77	90.62	89.61	99.06

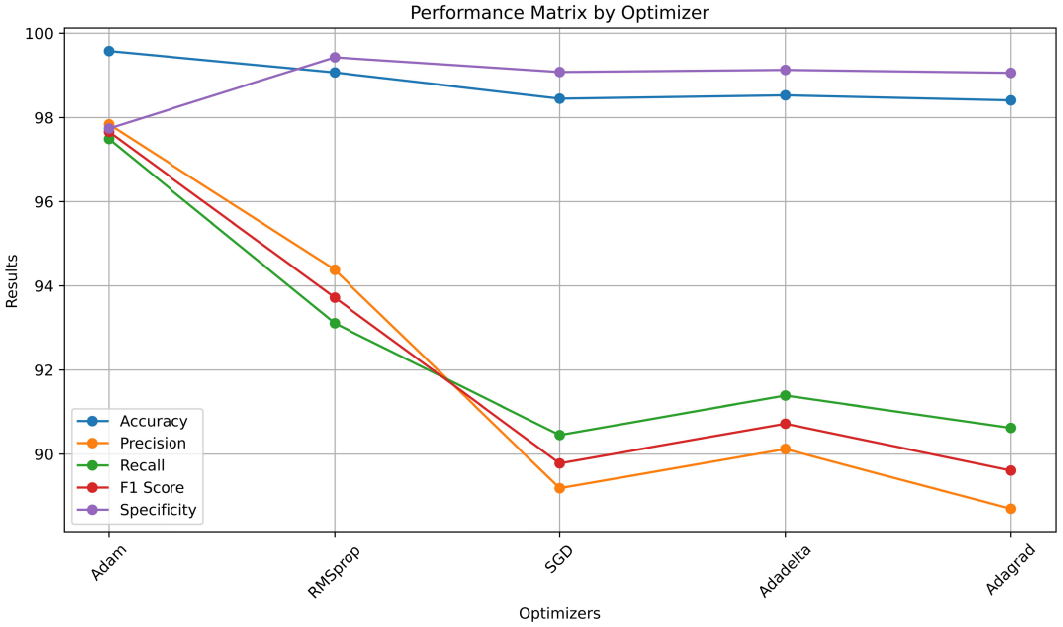

FIGURE 5. Graphical representation of the proposed QChPs-AE-LSTM model with various optimizers on the HAM10000 dataset.

the proposed model across various optimizers. The use of the Adam optimizer yielded the highest accuracy of 99.58%. Following closely, the RMSprop and Adadelta optimizer achieved 98.07% and 97.13% accuracies, respectively. However, the model exhibited relatively lower performance when utilizing the SGD and Adagrad optimizers, resulting in an accuracy of 94.50% and 93.23%, respectively. These results underscore the effectiveness and adaptability of the proposed methodology across various datasets and contexts.

The confusion matrix for the HAM10000 dataset, is illustrated in Fig. 6 (a-e). As depicted, the highest TP, reaching 99.35%, was achieved when utilizing the Adam optimizer, specifically for the Akiec class. For the BCC class, the model achieved a TP rate of 99.30%. For the Bkl, Df, Nv, Vasc, and Mel classes, the model achieved TP rates of 98.99%, 96.43%, 97.62%, 94.14%, and 96.62%, respectively. Fig. 6 (a-e) visually presents the confusion matrices of the proposed model corresponding to the Adam, Adagrad, RMSprop, SGD, and Adadelta optimizers, respectively.

B. COMPARISON WITH STATE OF THE ART

Skin cancers present a significant and widespread public health concern, demanding automated detection solutions. To address this challenge, contemporary research has harnessed the capabilities of machine learning and image processing techniques. Table 6 compares the performance outcomes of studies employing ISIC-2017 and HAM10000 datasets with the results achieved by our proposed model. In Table 6, it is observed that [51] reported an accuracy of 86.8% using the ISIC-2017 dataset and 88.6% with the HAM10000 dataset. Reference [52], on the other hand, obtained an accuracy of 96.5% using ISIC-2017 and 93.4%

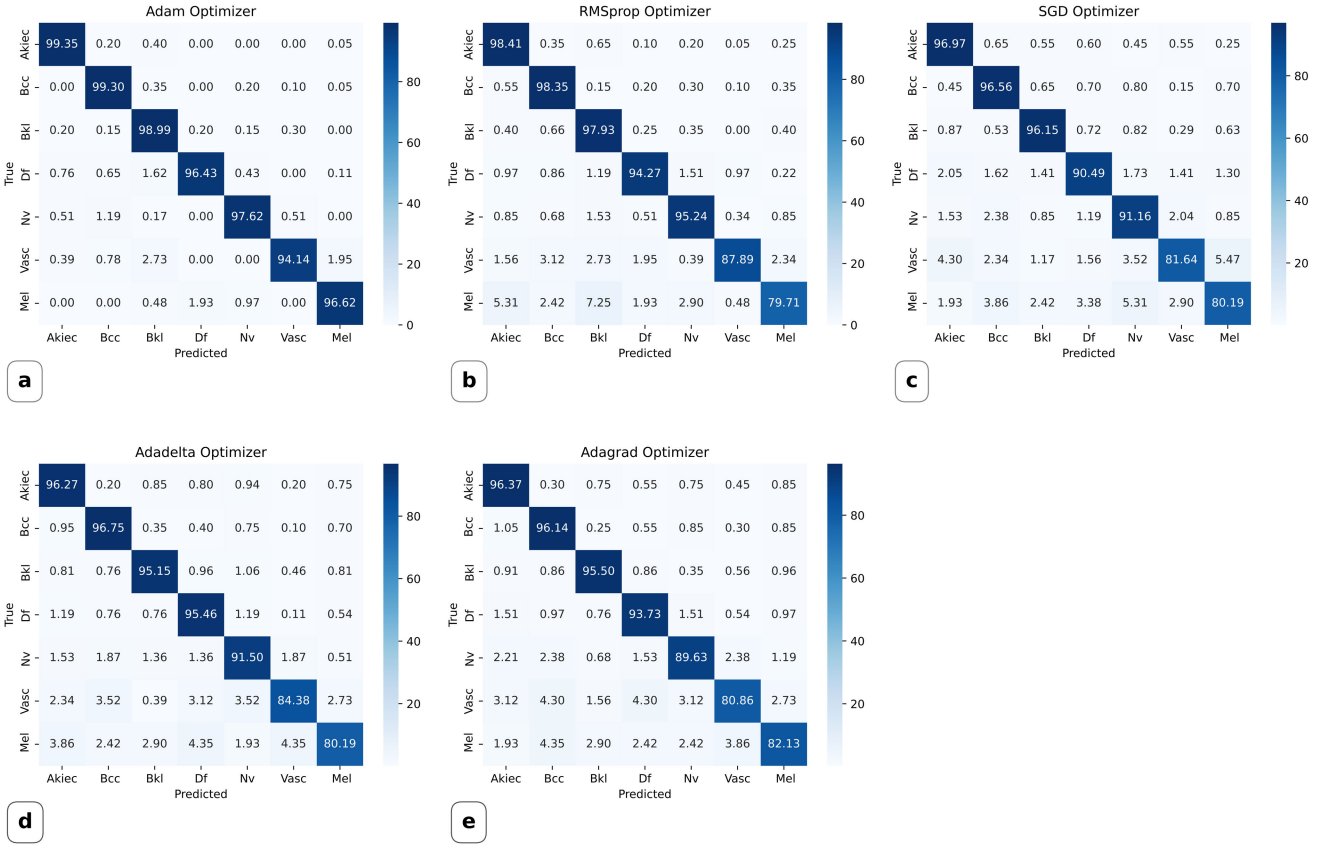

FIGURE 6. The confusion matrix displays classification results for (a) Adam optimizer, (b) RMSprop optimizer, (c) SGD optimizer, (d) Adadelta optimizer, and (e) Adagrad optimizer using HAM10000 dataset.

TABLE 6. Evaluating the performance of the proposed QChPs-AE-LSTM model compared to previous studies on ISIC2017 and HAM10000 datasets.

References	Methods	Dataset	Accuracy (%)	Precision (%)	Recall (%)	F1 Score (%)	Specificity (%)
[52]	ARL-CNN	ISIC-2017	86.8	–	–	–	86.7
		HAM10000	88.6	–	–	–	–
[53]	Soft Attention Coupling	ISIC-2017	71.1	–	–	–	71.1
		HAM10000	93.4	93.7	–	–	–
[54]	MMCA-KELM	HAM10000	90.7	–	–	–	–
[55]	W-net-Inception Resnet	ISIC-2017	96.97	95.71	–	–	97.87
[56]	DeepLoc	ISIC-2017	88.23	–	–	–	–
[51]	WT-DRNNet	ISIC-2017	96.91	96.43	–	–	97.68
		HAM10000	95.73	95.84	–	–	98.80
[46]	U-Net-CNN	HAM10000	97.6	–	–	–	–
[47]	Grasshopper-SURF-CNN	ISIC-2017	98.42	97.68	–	97.89	98.72
[48]	VGG, CapsNet, ResNet	ISIC-2019	93.5	–	87.0	–	94.0
[49]	DualAutoELM	HAM10000	97.66	97.68	97.59	–	–
	GWO-CNN	ISIC-2017	86.68	86.75	86.62	–	–
[50]		ISIC-2017	94.5	–	–	–	–
Proposed	QChPs-AE-LSTM	ISIC-2017	98.87	98.23	98.26	98.24	98.16
		HAM10000	99.58	97.84	97.49	97.66	97.74

using HAM10000. Reference [53] achieved an accuracy of 90.7% with the HAM10000 dataset. In comparison, [54] and [55], using the ISIC-2017 dataset, achieved 96.97% and 88.23% accuracy, respectively. Reference [50] conducted a comprehensive study using both datasets, obtaining an accuracy of 96.91% with ISIC-2017 and 95.73% with HAM10000. Reference [45] reported an accuracy of 97.6% using the HAM10000 dataset, while [46] achieved 98.42% accuracy with the ISIC 2017 dataset. Reference [47], using the ISIC-2019 dataset, attained an accuracy of 93.5%. Similarly, in line with our study, [48] used both the ISIC-2017 and HAM10000 datasets, achieving 97.66% for HAM10000 and 86.68% for ISIC-2017. Lastly, [49] obtained an accuracy of 94.5% using the ISIC-2017 dataset.

In contrast, our proposed model exhibits remarkable accuracy, reaching 98.87% with the ISIC-2017 dataset and an even higher accuracy of 99.58% with the HAM10000 dataset. These compelling results underscore the effectiveness of

our proposed model across both datasets and outperformed previous studies. The experimental results provide substantial evidence that our proposed QChPs-AE-LSTM model significantly enhances classification performance, particularly in terms of accuracy.

C. LIMITATION OF THE CURRENT STUDY

One notable limitation of this study is the significant computational time required. The proposed model follows a multi-step process, starting with image preprocessing, then performing feature extraction using the QChPs model, and finally passing the features through AE for refinement and dimensionality reduction. While these operations are essential to the model's effectiveness, they demand substantial computational resources and time.

V. CONCLUSION AND FUTURE WORK

In conclusion, the critical issue of incorrect or delayed cancer diagnoses, which often lead to patient fatalities, highlights the importance of early and accurate detection. Traditional manual methods for SC detection have frequently proven inadequate, resulting in lower detection rates, increased burdens on medical professionals, and higher costs and time commitments. To address these challenges, this study introduced a novel multi-stage model for precise skin lesion classification. The proposed approach begins with advanced preprocessing techniques to enhance image quality, removing unwanted elements such as hair and emphasizing fine details. Quantum Chebyshev polynomials are used for initial feature extraction, followed by further refinement and dimensionality reduction using an Autoencoder. These features are then classified using an LSTM network. The model's performance was evaluated using five distinct optimizers—Adam, RMSprop, SGD, Adadelta, and Adagrad—across two datasets: ISIC 2017 and HAM10000.

For the ISIC-2017 dataset, the model achieved excellent results, with accuracy, precision, recall, F1-score, and specificity reaching 98.87%, 98.23%, 98.26%, 98.24%, and 98.16%, respectively, using the Adam optimizer. Similarly, the HAM10000 dataset yielded remarkable metrics of 99.58%, 97.84%, 97.49%, 97.66%, and 97.74%, respectively. Comparative analysis shows that the proposed model outperforms prior methods, demonstrating its potential as a valuable tool for medical professionals in automating SC classification based on skin lesion images.

Future work will focus on enhancing the feature extraction process and exploring innovative methods to reduce computational time, making the model more efficient and practical. These improvements will benefit both patients and healthcare providers in the fight against SC.

DECLARATION OF INTERESTS

The authors declare that this manuscript is original, has not been published before, and is not currently being considered for publication elsewhere.

REFERENCES

[1] J. Reichrath, U. Leiter, T. Eigentler, and C. Garbe, "Epidemiology of skin cancer," in *Sunlight, Vitamin D and Skin Cancer*. Springer, 2014, pp. 120–140.

[2] J. Saeed and S. Zeebaree, "Skin lesion classification based on deep convolutional neural networks architectures," *J. Appl. Sci. Technol. Trends*, vol. 2, no. 1, pp. 41–51, Mar. 2021.

[3] M. Janda and H. P. Soyer, "Using advances in skin imaging technology and genomics for the early detection and prevention of melanoma," *Dermatology*, vol. 235, no. 1, pp. 1–3, 2019.

[4] N. N. Sultana and N. B. Puhan, "Recent deep learning methods for melanoma detection: A review," in *Proc. Math. Computing: 4th Int. Conf. (ICMC)*, vol. 834, D. Ghosh, D. Giri, R. N. Mohapatra, E. Savas, K. Sakurai, and L. P. Singh, Eds. Singapore: Springer, Jan. 2018, pp. 118–132.

[5] M. A. Anjum, J. Amin, M. Sharif, H. U. Khan, M. S. A. Malik, and S. Kadry, "Deep semantic segmentation and multi-class skin lesion classification based on convolutional neural network," *IEEE Access*, vol. 8, pp. 129668–129678, 2020.

[6] M. A. Khan, S. Kadry, M. Alhaisoni, Y. Nam, Y. Zhang, V. Rajinikanth, and M. S. Sarfraz, "Computer-aided gastrointestinal diseases analysis from wireless capsule endoscopy: A framework of best features selection," *IEEE Access*, vol. 8, pp. 132850–132859, 2020.

[7] D. K. Iakovidis, S. V. Georgakopoulos, M. Vasilakakis, A. Koulaouzidis, and V. P. Plagianakos, "Detecting and locating gastrointestinal anomalies using deep learning and iterative cluster unification," *IEEE Trans. Med. Imag.*, vol. 37, no. 10, pp. 2196–2210, Oct. 2018.

[8] D. Schadendorf, A. C. J. van Akkooi, C. Berking, K. G. Griewank, R. Gutzmer, A. Hauschild, A. Stang, A. Roesch, and S. Ugurel, "Melanoma," *Lancet*, vol. 392, no. 10151, pp. 971–984, Sep. 2018.

[9] V. K. Singh, M. Abdel-Nasser, H. A. Rashwan, F. Akram, N. Pandey, A. Lalande, B. Presles, S. Romani, and D. Puig, "FCA-net: Adversarial learning for skin lesion segmentation based on multi-scale features and factorized channel attention," *IEEE Access*, vol. 7, pp. 130552–130565, 2019.

[10] M. E. Vestergaard, P. Macaskill, P. E. Holt, and S. W. Menzies, "Dermoscopy compared with naked eye examination for the diagnosis of primary melanoma: A meta-analysis of studies performed in a clinical setting," *Brit. J. Dermatol.*, vol. 159, no. 3, pp. 669–676, 2008.

[11] C. Barata, M. E. Celebi, and J. S. Marques, "A survey of feature extraction in dermoscopy image analysis of skin cancer," *IEEE J. Biomed. Health Inf.*, vol. 23, no. 3, pp. 1096–1109, May 2019.

[12] D. N. A. Ningrum, S.-P. Yuan, W.-M. Kung, C.-C. Wu, I.-S. Tzeng, C.-Y. Huang, J. Y.-C. Li, and Y.-C. Wang, "Deep learning classifier with Patient's metadata of dermoscopic images in malignant melanoma detection," *J. Multidisciplinary Healthcare*, vol. Volume 14, pp. 877–885, Apr. 2021.

[13] A. Masood and A. A. Al-Jumaily, "Computer aided diagnostic support system for skin cancer: A review of techniques and algorithms," *Int. J. Biomed. Imag.*, vol. 2013, pp. 1–22, Jul. 2013.

[14] A. Mobiny, A. Singh, and H. Van Nguyen, "Risk-aware machine learning classifier for skin lesion diagnosis," *J. Clin. Med.*, vol. 8, no. 8, p. 1241, Aug. 2019.

[15] M. A. Kassem, K. M. Hosny, and M. M. Fouad, "Skin lesions classification into eight classes for ISIC 2019 using deep convolutional neural network and transfer learning," *IEEE Access*, vol. 8, pp. 114822–114832, 2020.

[16] J. Szaleniec, M. Szaleniec, P. Stręk, A. Boroń, K. Jabłońska, J. Gawlik, and J. Składzień, "Outcome prediction in endoscopic surgery for chronic rhinosinusitis—A multidimensional model," *Adv. Med. Sci.*, vol. 59, no. 1, pp. 13–18, Mar. 2014.

[17] H. K. Gajera, D. R. Nayak, and M. A. Zaveri, "A comprehensive analysis of dermoscopy images for melanoma detection via deep CNN features," *Biomed. Signal Process. Control*, vol. 79, Jan. 2023, Art. no. 104186.

[18] M. Fatima, M. A. Khan, S. Shaheen, N. A. Almujally, and S. Wang, "$B^2C^3NetF^2$: Breast cancer classification using an end-to-end deep learning feature fusion and satin bowerbird optimization controlled Newton Raphson feature selection," *CAAI Trans. Intell. Technol.*, vol. 8, no. 4, pp. 1374–1390, Dec. 2023.

[19] S. Chaudhury, K. Sau, M. A. Khan, and M. Shabaz, "Deep transfer learning for IDC breast cancer detection using fast AI technique and sqeezenet architecture," *Math. Biosciences Eng.*, vol. 20, no. 6, pp. 10404–10427, 2023.

[20] K. Jabeen, M. A. Khan, J. Balili, M. Alhaisoni, N. A. Almujally, H. Alrashidi, U. Tariq, and J.-H. Cha, "BC^{2}NetRF: Breast cancer classification from mammogram images using enhanced deep learning features and equilibrium-jaya controlled regula falsi-based features selection," *Diagnostics*, vol. 13, no. 7, p. 1238, Mar. 2023.

[21] H. M. Ünver and E. Ayan, "Skin lesion segmentation in dermoscopic images with combination of YOLO and GrabCut algorithm," *Diagnostics*, vol. 9, no. 3, p. 72, Jul. 2019.

[22] S. Ayas, "Multiclass skin lesion classification in dermoscopic images using swin transformer model," *Neural Comput. Appl.*, vol. 35, no. 9, pp. 6713–6722, Mar. 2023.

[23] N. Nida, A. Irtaza, A. Javed, M. H. Yousaf, and M. T. Mahmood, "Melanoma lesion detection and segmentation using deep region based convolutional neural network and fuzzy C-means clustering," *Int. J. Med. Inf.*, vol. 124, pp. 37–48, Apr. 2019.

[24] K. Polat and K. Onur Koc, "Detection of skin diseases from dermoscopy image using the combination of convolutional neural network and one-versus-all," *J. Artif. Intell. Syst.*, vol. 2, no. 1, pp. 80–97, 2020.

[25] M. Kumar, M. Alshehri, R. AlGhamdi, P. Sharma, and V. Deep, "A DE-ANN inspired skin cancer detection approach using fuzzy C-means clustering," *Mobile Netw. Appl.*, vol. 25, no. 4, pp. 1319–1329, Aug. 2020.

[26] A. A. Adegun and S. Viriri, "FCN-based DenseNet framework for automated detection and classification of skin lesions in dermoscopy images," *IEEE Access*, vol. 8, pp. 150377–150396, 2020.

[27] P. N. Srinivasu, J. G. Sivasai, M. F. Ijaz, A. K. Bhoi, W. Kim, and J. J. Kang, "Classification of skin disease using deep learning neural networks with MobileNet V2 and LSTM," *Sensors*, vol. 21, no. 8, p. 2852, Apr. 2021.

[28] A. Mahbod, G. Schaefer, C. Wang, G. Dorffner, R. Ecker, and I. Ellinger, "Transfer learning using a multi-scale and multi-network ensemble for skin lesion classification," *Comput. Methods Programs Biomed.*, vol. 193, Sep. 2020, Art. no. 105475.

[29] N. Zhang, Y.-X. Cai, Y.-Y. Wang, Y.-T. Tian, X.-L. Wang, and B. Badami, "Skin cancer diagnosis based on optimized convolutional neural network," *Artif. Intell. Med.*, vol. 102, Jan. 2020, Art. no. 101756.

[30] N. Hameed, A. M. Shabut, M. K. Ghosh, and M. A. Hossain, "Multi-class multi-level classification algorithm for skin lesions classification using machine learning techniques," *Expert Syst. Appl.*, vol. 141, Mar. 2020, Art. no. 112961.

[31] M. K. Hasan, L. Dahal, P. N. Samarakoon, F. I. Tushar, and R. Martí, "DSNet: Automatic dermoscopic skin lesion segmentation," *Comput. Biol. Med.*, vol. 120, May 2020, Art. no. 103738.

[32] K. M. Hosny, M. A. Kassem, and M. M. Fouad, "Classification of skin lesions into seven classes using transfer learning with AlexNet," *J. Digit. Imag.*, vol. 33, no. 5, pp. 1325–1334, Oct. 2020.

[33] S. Chatterjee, D. Dey, and S. Munshi, "Integration of morphological preprocessing and fractal based feature extraction with recursive feature elimination for skin lesion types classification," *Comput. Methods Programs Biomed.*, vol. 178, pp. 201–218, Sep. 2019.

[34] P. M. M. Pereira, R. Fonseca-Pinto, R. P. Paiva, P. A. A. Assuncao, L. M. N. Tavora, L. A. Thomaz, and S. M. M. Faria, "Skin lesion classification enhancement using border-line features—The melanoma vs nevus problem," *Biomed. Signal Process. Control*, vol. 57, Mar. 2020, Art. no. 101765.

[35] J. L. Garcia-Arroyo and B. Garcia-Zapirain, "Segmentation of skin lesions in dermoscopy images using fuzzy classification of pixels and histogram thresholding," *Comput. Methods Programs Biomed.*, vol. 168, pp. 11–19, Jan. 2019.

[36] I. Zaqout, "Diagnosis of skin lesions based on dermoscopic images using image processing techniques," in *Pattern Recognition-Selected Methods AApplications*, vol. 1320. Poland: IntechOpen, 2019. [Online]. Available: https://www.intechopen.com/books/7405

[37] M. A. Khan, T. Akram, Y.-D. Zhang, and M. Sharif, "Attributes based skin lesion detection and recognition: A mask RCNN and transfer learning-based deep learning framework," *Pattern Recognit. Lett.*, vol. 143, pp. 58–66, Mar. 2021.

[38] M. A. Khan, M. Y. Javed, M. Sharif, T. Saba, and A. Rehman, "Multi-model deep neural network based features extraction and optimal selection approach for skin lesion classification," in *Proc. Int. Conf. Comput. Inf. Sci. (ICCIS)*, Apr. 2019, pp. 1–7.

[39] M. A. Khan, Y.-D. Zhang, M. Sharif, and T. Akram, "Pixels to classes: Intelligent learning framework for multiclass skin lesion localization and classification," *Comput. Electr. Eng.*, vol. 90, Mar. 2021, Art. no. 106956.

[40] A. Sáez, J. Sánchez-Monedero, P. A. Gutiérrez, and C. Hervás-Martínez, "Machine learning methods for binary and multiclass classification of melanoma thickness from dermoscopic images," *IEEE Trans. Med. Imag.*, vol. 35, no. 4, pp. 1036–1045, Apr. 2016.

[41] Z. Yu, X. Jiang, F. Zhou, J. Qin, D. Ni, S. Chen, B. Lei, and T. Wang, "Melanoma recognition in dermoscopy images via aggregated deep convolutional features," *IEEE Trans. Biomed. Eng.*, vol. 66, no. 4, pp. 1006–1016, 2019.

[42] V. Anand, S. Gupta, A. Altameem, S. R. Nayak, R. C. Poonia, and A. K. J. Saudagar, "An enhanced transfer learning based classification for diagnosis of skin cancer," *Diagnostics*, vol. 12, no. 7, p. 1628, Jul. 2022.

[43] V. Anand, S. Gupta, D. Koundal, S. R. Nayak, J. Nayak, and S. Vimal, "Multi-class skin disease classification using transfer learning model," *Int. J. Artif. Intell. Tools*, vol. 31, no. 2, Mar. 2022, Art. no. 2250029.

[44] V. Anand, S. Gupta, and D. Koundal, "Detection and classification of skin disease using modified mobilenet architecture," *ECS Trans.*, vol. 107, no. 1, pp. 5059–5067, Apr. 2022.

[45] V. Anand, S. Gupta, D. Koundal, and K. Singh, "Fusion of U-Net and CNN model for segmentation and classification of skin lesion from dermoscopy images," *Expert Syst. Appl.*, vol. 213, Mar. 2023, Art. no. 119230.

[46] P. Thapar, M. Rakhra, M. Alsaadi, A. Quraishi, A. Deka, and J. V. N. Ramesh, "A hybrid grasshopper optimization algorithm for skin lesion segmentation and melanoma classification using deep learning," *Healthcare Anal.*, vol. 5, Jun. 2024, Art. no. 100326.

[47] A. Imran, A. Nasir, M. Bilal, G. Sun, A. Alzahrani, and A. Almuhaimeed, "Skin cancer detection using combined decision of deep learners," *IEEE Access*, vol. 10, pp. 118198–118212, 2022.

[48] R. Maurya, S. Mahapatra, M. K. Dutta, V. P. Singh, M. Karnati, G. Sahu, and N. N. Pandey, "Skin cancer detection through attention guided dual autoencoder approach with extreme learning machine," *Sci. Rep.*, vol. 14, no. 1, p. 17785, Aug. 2024.

[49] N. Saleh, M. A. Hassan, and A. M. Salaheldin, "Skin cancer classification based on an optimized convolutional neural network and multicriteria decision-making," *Sci. Rep.*, vol. 14, no. 1, p. 17323, Jul. 2024.

[50] F. Alenezi, A. Armghan, and K. Polat, "Wavelet transform based deep residual neural network and ReLU based extreme learning machine for skin lesion classification," *Expert Syst. Appl.*, vol. 213, Mar. 2023, Art. no. 119064.

[51] J. Zhang, Y. Xie, Y. Xia, and C. Shen, "Attention residual learning for skin lesion classification," *IEEE Trans. Med. Imag.*, vol. 38, no. 9, pp. 2092–2103, Sep. 2019.

[52] S. K. Datta, M. A. Shaikh, S. N. Srihari, and M. Gao, "Soft attention improves skin cancer classification performance," in *Proc. 4th Int. Workshop (iMIMIC), 1st Int. Workshop*, Strasbourg, France. Cham, Switzerland: Springer, Sep. 27, 2021, pp. 13–23.

[53] M. A. Khan, M. Sharif, T. Akram, R. Damaševič ius, and R. Maskeliūnas, "Skin lesion segmentation and multiclass classification using deep learning features and improved moth flame optimization," *Diagnostics*, vol. 11, no. 5, p. 811, Apr. 2021.

[54] S. Khouloud, M. Ahlem, T. Fadel, and S. Amel, "W-net and inception residual network for skin lesion segmentation and classification," *Int. J. Speech Technol.*, vol. 52, no. 4, pp. 3976–3994, Mar. 2022.

[55] O. Z. Kraus, B. T. Grys, J. Ba, Y. Chong, B. J. Frey, C. Boone, and B. J. Andrews, "Automated analysis of high-content microscopy data with deep learning," *Mol. Syst. Biol.*, vol. 13, no. 4, p. 924, Apr. 2017.

[56] P. Tschandl, C. Rosendahl, and H. Kittler, "The HAM10000 dataset, a large collection of multi-source dermatoscopic images of common pigmented skin lesions," *Sci. Data*, vol. 5, no. 1, pp. 1–9, Aug. 2018.

[57] Z. E. Diame, M. N. Al-Berry, M. A.-M. Salem, and M. Roushdy, "Autoencoder performance analysis of skin lesion detection," *J. Southwest Jiaotong Univ.*, vol. 56, no. 6, pp. 937–947, Dec. 2021.

FARHATULLAH received the B.S. degree in computer science and information technology from the University of Malakand and the master's degree from the Department of Computer Science, Abasyn University, Peshawar, Pakistan. He is currently pursuing the Ph.D. degree with the School of Computer Science, China University of Geosciences, Wuhan. His current research interests include medical image processing, Alzheimer's disease, neurological disorders, skin disease, and tractography.

XIN CHEN (Member, IEEE) received the B.S. degree in industrial automation and the M.S. degree in control theory and control engineering from Central South University, Changsha, China, in 1999 and 2002, respectively, and the Ph.D. degree in mechanical and electrical engineering from the National Ministry of Education, University of Macao, Macau, SAR, China, in 2007. In 2011, he finished postdoctoral research in control science and engineering with Central South University. In 2014, he joined China University of Geosciences, Wuhan, China, where he is currently a Professor with the School of Automation. From 2018 to 2019, he was a Visiting Scholar with the Department of Electrical and Computer Engineering, University of Alberta, Edmonton, AB, Canada. His current research interests include multiagent systems, robotics, process control, and intelligent control.

DEZE ZENG (Senior Member, IEEE) is currently a Full Professor with the School of Computer Science, China University of Geosciences, Wuhan, China. His main current research interests include edge computing and cloud computing. He has authored three books and over 120 papers in refereed journals and conferences in these areas. He also received five best paper awards from IEEE/ACM conferences and journals. He serves as the Specialty Chief Editor for *Frontiers in Internet of Things* and on editorial boards for IEEE TRANSACTIONS ON SUSTAINABLE COMPUTING, *Journal of Network and Computer Applications*, *Frontiers of Computer Science*, and *Open Journal of Computer Society*. He has been on the organization or program committees of many international conferences. He is a Distinguished Member of CCF.

JIAFENG XU (Student Member, IEEE) received the B.S. degree in electrical engineering from Wuhan University of Technology, in 2017. He is currently pursuing the Ph.D. degree in control engineering with the School of Automation, China University of Geosciences, Wuhan, China. His current research interests include geo-drilling technology, evolutionary computation, and complex system modeling.

RAB NAWAZ (Member, IEEE) received the bachelor's degree in electronic engineering from International Islamic University, Islamabad, Pakistan, the master's degree in electrical engineering from NUST University, Islamabad, and the Ph.D. degree in engineering from Universiti Tunku Abdul Rahman (UTAR), Malaysia. He is currently a Lecturer with the School of Computer Science and Electronic Engineering, University of Essex. Before joining the University of Essex, he was a Postdoctoral Research Associate with the Department of Biomedical Engineering, University of Glasgow, Scotland. Previously, he was a Visiting Research Scholar with the University of Graz, Austria. During his professional career, he has performed cutting-edge research in the fields of biomedical engineering, BCI, and machine learning. He has co-authored quality research papers, including in leading international journals and peer-reviewed international conference proceedings. He has also received the best paper awards at two international conferences.

RAHMAT ULLAH (Member, IEEE) received the master's degree in software engineering from COMSATS University Islamabad, Pakistan, and the Ph.D. degree from the School of Engineering, The University of Edinburgh, Edinburgh, U.K. He was a Research and Development Associate with the Faculty of Computing, Engineering and Science, University of South Wales, U.K. He is currently a Lecturer with the School of Computer Science and Electronic Engineering, University of Essex, U.K. His research interests include biomedical signal processing, microwave imaging, software engineering, machine learning, and digital health.